A Dual-Functional Massive MIMO OFDM Communication and Radar Transmitter Architecture

Murat Temiz, *Student Member, IEEE*, Emad Alsusa, *Senior Member, IEEE,* and Mohammed W. Baidas, *Senior Member, IEEE*

***Abstract*—In this study, a dual-functional radar and communication (RadCom) system architecture is proposed for application at base-stations (BSs), or access points (APs), for simultaneously communicating with multiple user equipments (UEs) and sensing the environment. Specifically, massive multiple-input multiple-output (mMIMO) communication and orthogonal frequency-division multiplexing (OFDM)-based MIMO radar are considered with the objective to jointly utilize channel diversity and interference. The BS consists of a mMIMO antenna array, and radar transmit and receive antennas. Employing OFDM waveforms for the radar allows the BS to perform channel state information (CSI) estimation for the mMIMO and radar antennas simultaneously. The acquired CSI is then exploited to predict the radar signals received by the UEs. While the radar transmits an OFDM waveform for detecting possible targets in range, the communication system beamforms to the UEs taking into account the predicted radar interference. To further enhance the capacity of the communication system, an optimum radar waveform is designed. Moreover, the network capacity is mathematically analyzed and verified by simulations. The results show that the proposed RadCom can achieve higher capacity than conventional mMIMO systems by utilizing the radar interference while simultaneously detecting targets.**

***Index Terms*—Interference management, massive MIMO, OFDM radar, RadCom, precoder design, waveform design**

I. Introduction

The relative success of current wireless networks has raised the expectations from next-generation networks (5G and beyond) such as supporting a massive number of devices, reducing latency or being able to detect targets present in the propagation environment. Meanwhile, radar systems and communication networks have been gradually converging in the frequency spectrum due to the increasing demands on bandwidth by various data hungry communication applications [1]. For example, autonomous driving applications require the vehicles to communicate with each other (vehicle-to-vehicle - V2V) and their surroundings (vehicle-to-everything - V2X), while sensing the road conditions to provide safer and better driving. Such applications require a substantial amount of bandwidth of an increasingly congested spectrum [2]. Therefore, this study presents a joint massive MIMO radar-communication (RadCom) platform, where the radar operates simultaneously with the communication downlink using the same time-frequency resources.

M. Temiz and E. Alsusa are with the Department of Electrical and Electronic Engineering, University of Manchester, Manchester, UK and M. W. Baidas is with the Department of Electrical Engineering, Kuwait University, Kuwait. {e-mail:{murat.temiz, e.alsusa}@manchester.ac.uk, m.baidas@ku.edu.kw}

Several studies have recently investigated the capacity of communication networks in the presence of radar interference and have considered various methods to jointly enhance their performance [3]–[9]. For example, one of the approaches is forcing a MIMO radar to beamform its waveform into the null space of the radar-communication interference channel [3], [5]. Another technique for the cooperation between MIMO communication and MIMO matrix completion (MIMO-MC) radar was introduced in [6] where both radar and communication systems precode their respective signals to avoid interfering with each other. To reduce the interference between radar and communication systems, a robust OFDM radar waveform and radar transmit power minimization have been proposed in [10], where scattered communication signals from the targets are utilized for sensing. Another approach considered utilizing the inter-user interference as constructive interference at the UEs to increase the received communication power and alleviate the radar interference [11]. The studies about the interaction between these two systems from simply sharing the same spectrum to designing cooperatively operating RadCom systems have been categorically reviewed in [12] which also presented several applications where co-existence or co-operation of radar and communication systems are inevitable, such as in vehicular communication networks or commercial flight control systems. From another point of view, these two systems can be developed to operate on the same hardware. Several studies have recently considered developing dual-functional RadCom systems [8], [13]–[16]. Liu $et\ al.$ compared the cases in which the antenna array is shared for MIMO communications and MIMO radar, and when separate antenna arrays are employed for the two systems [13]. When using separate antennas, the radar signals are forced into the null spaces of the communication interference channel. While, for the shared antenna deployment, the targets of interest are recognized as virtual UEs to allow radar beamforming towards them, though, this method requires foreknowledge of the target locations. It was shown that shared deployment provides superior network capacity. The authors in [14] considered using radar pulses as downlink communication frames to communicate with downlink UEs. Also, in [15], a system architecture based on multibeam waveforms was proposed, while in [16] antenna selection algorithms are introduced for MIMO RadCom to transmit signals encapsulating communication and radar symbols. Moreover, joint resource and power allocations were considered to enhance energy efficiency in RadCom, while satisfying certain data-rate and target-detection requirements [17]–[19]. For example, OFDM waveforms were considered to

achieve such enhancement by allocating different subcarriers to the communication and radar parts, but this reduces the available bandwidth to each system, [8].

In contrast to previous studies, in this paper, we propose a precoding-based transmitter for dual-functional MIMO OFDM RadCom, where both the communication and radar systems transmit their respective waveforms by occupying the entire available bandwidth at the same time. Moreover, the radar part can emit powerful waveforms and the communication part communicates with multiple downlink UEs while utilizing the radar interference. The proposed method predicts the radar interference at the UEs by exploiting the estimated CSI and constructs a precoder matrix that can lead to constructive radar interference at all UEs. The main contributions of this work can be summarized as:

- Propose a novel massive MIMO OFDM RadCom transmitter architecture that can exploit the radar interference while providing downlink communications to multiple users, and radar sensing.
- Present optimum waveform design for the radar part of the proposed system to enhance the communication and radar performance.
- Provid analytical channel capacity derivations of the proposed transmitter architecture with perfectly and imperfectly estimated CSI, and verify them by simulations.

In the rest of this paper, Section II introduces the system model, while Section III presents the precoder design. Section IV proposes an optimum radar waveform design technique. The channel capacity analysis and the performance of radar detection are presented in Sections V, and VI, respectively. Section VII presents the simulations results and discussions. Finally, Section VIII draws the conclusions.

Notation: Throughout the paper, the following notation is used. Bold uppercase letters (e.g. $\mathbf{H}$) indicate matrices while bold lowercase letters (e.g. $\mathbf{h}$) indicate vectors. Superscript $^*, ^T, ^H$ indicate conjugate, transpose and Hermitian transpose, respectively. Subscript $_{com}$ and $_{rad}$ symbolize that the corresponding parameter is related to communication or radar systems (e.g. $\mathbf{H}_{com}$ and $\mathbf{H}_{rad}$), respectively. $\mathbb{E}[.]$ and $tr[.]$ denote the expectation operator and the trace of a matrix, respectively. The absolute value, Euclidean norm and Frobenius norm operators are denoted by $|.|$, $\|.\|$ and $\|.\|_F$, respectively.

II. System Model

Fig. 1 illustrates the system model in which massive MIMO downlink communication and transmission and reception of omnidirectional OFDM radar waveforms are simultaneously accomplished by the RadCom BS. Fig. 2 illustrates the block diagram of the proposed BS/AP architecture, where firstly, the radar waveform and communication precoder matrices are constructed, followed by the inverse fast Fourier transform (IFFT) before the signals are conveyed to the antennas via digital-to-analog converters (DACs) and the transmitter's (Tx) RF chains. On the radar receiver side, the reflected signals are converted to baseband via the analog-to-digital converters (ADCs). Subsequently, the digital canceller estimates the self-interference from the transmit antennas and eliminates it

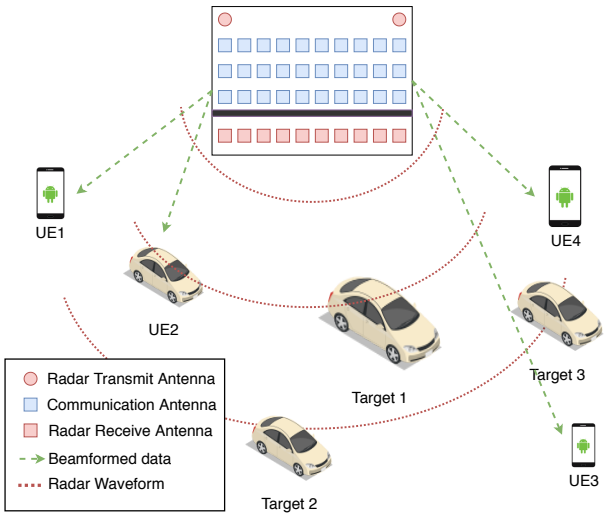

Fig. 1. A dual-functional BS which beamforms communication symbols towards the downlink UEs while emitting a radar waveform into all directions.

before the FFT process. After which, the range-velocity and range-angle profiles of the targets are estimated. The BS architecture under consideration is composed of an antenna array consisting of M elements for mMIMO communication with K UEs, P antennas for transmitting orthogonal MIMO radar waveforms, and a uniform linear antenna (ULA) array with Q antennas for receiving the radar returns. The separation between two adjacent radar receive antennas or two adjacent communication antennas is $d_Q = \lambda/2$, and between the two adjacent radar transmit antennas is $(Q-1)\,d_Q$. Time division duplex (TDD) is selected as the operation mode of the system as illustrated in Fig. 3, where the duration of each TDD frame, $\Delta t = t_c + t_d + t_u$, includes CSI estimation, downlink and uplink durations, respectively, and it is shorter than the coherence time, τ, i.e. $\Delta t < \tau$. Due to the reciprocity of the channels, only uplink CSI estimation is required at the beginning of each coherence block, [20].

The communication and radar operations are synchronized such that the radar transmit antennas emit the radar waveform, while the radar receive antennas receive the echos from the targets during the communication downlink[1]. Note that while communication signals are beamformed towards the desired UEs by exploiting spatial diversity, the radar signals must be emitted into all directions to cover a wide range of area for sensing. This study focuses only on downlink communication and target detection simultaneously. Hence, uplink communication is not considered. However, during uplink, all radar transmit and receive antennas can be utilized for uplink communication to enhance the uplink capacity. Moreover, it is also possible to perform target detection during uplink by employing successive interference cancellation [21].

[1]The radar Rx must operate slightly longer than the Tx to acquire all the reflected signals. However, this is relatively short compared to the symbols. Since the radar range considered is 200m, the maximum round-trip is 1.33 μs, which is less than the downlink and symbol durations, i.e., $t_d = 100$ μs and $t_{sym} = 7.66$ μs, and is equal to $t_{cp} = 1.33$ μs, as given in Table II.

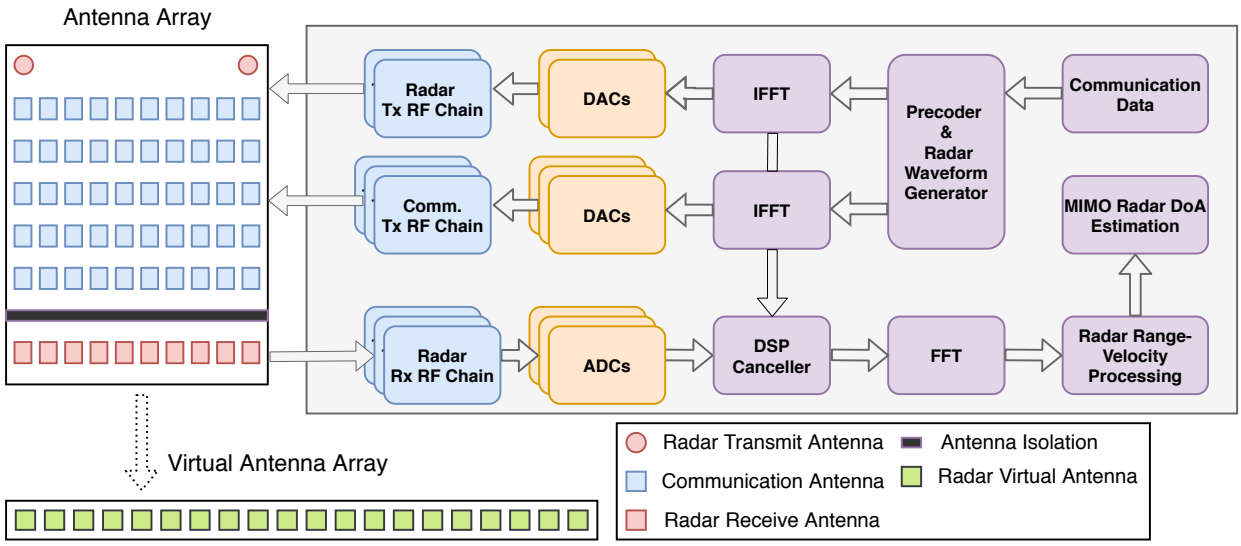

Fig. 2. A prototype downlink RadCom architecture with communication and radar antennas on the left. The virtual antenna array given on the left-bottom is obtained by MIMO radar processing of two transmit antennas from the radar receive antennas. The uplink communication blocks are not shown here.

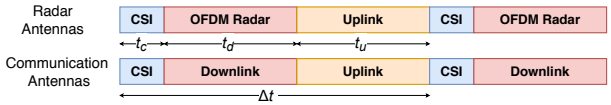

Fig. 3. Synchronized RadCom TDD operation mode .

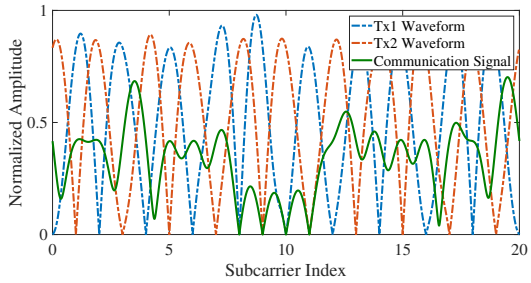

Fig. 4. Arbitrary OFDM waveforms transmitted by two radar antennas and OFDM communication symbols transmitted by one communication antenna.

A. OFDM MIMO Radar Model

A continuous-wave OFDM radar is considered for radar sensing since vehicular radars must be able to detect targets up to 200 m [2]. A modulation symbol-based OFDM radar processing is employed as it has a higher peak-to-side-lobe ratio compared to correlation-based radar processing [22]. Estimation of the target features using this radar is similar to the channel estimation widely used in MIMO-OFDM communication systems as explained in Section VI. The foremost advantages of employing OFDM in RadCom systems are that the CSI estimation can be simultaneously performed for the radar and communication antennas, and only a narrow frequency band (one subcarrier) can be focused on to alleviate the direct-coupling and cross-system interference. MIMO radar systems transmit orthogonal waveforms via each transmit antenna and the signals reflected off the targets are generally received by an antenna array [23]. Having separated radar transmit antennas transmitting orthogonal waveforms, a virtual antenna array consisting of $P \times Q$ elements can be constructed as shown in Fig. 2 by exploiting the diversity of the transmitted orthogonal radar waveforms [8]. This virtual array provides a better angle resolution than the real array. To ensure orthogonality between the radar transmit antennas, the OFDM radar signals transmitted by the radar antennas are interleaved in the frequency domain as discussed in [24]. Fig. 4 illustrates the interleaved OFDM waveforms by two radar antennas and an OFDM communication signal transmitted by only one antenna element of the array, which overlaps with the radar spectrum. The interleaved OFDM radar waveform can be briefly explained as follows. The μth symbol of the OFDM waveform transmitted by a radar antenna on the nth subcarrier is denoted by $\Omega_{\mu,n}(t)$, which is randomly drawn from a normalized M-PSK or M-QAM constellation. Moreover, $f_c+n\Delta f$ denotes the frequency of the nth subcarrier, Δf denotes the subcarrier spacing and t denotes the sampling time. Each OFDM symbol has a duration of $t_o = t_{sym}+t_{cp}$ consisting of the symbol and cyclic-prefix (CP), respectively. Accordingly, during each downlink subframe, $N_{sym} = t_d/t_o$ symbols are transmitted. Assuming that the radar has two transmit antennas such that all subcarriers are occupied by two antennas in an interleaved way as shown in Fig. 4. Accordingly, the OFDM waveform matrix, $\mathbf{S}_p \in \mathbb{C}^{V\times N_c/P}$, transmitted by the pth radar transmit antenna (for $p \in \{1,2\}$) can be expressed as

$$\mathbf{S}_p(t)=\begin{pmatrix} \Omega_{1,p}(t) & \Omega_{1,p+2}(t) & \cdots & \Omega_{1,p+N_c-2}(t) \\ \Omega_{2,p}(t) & \Omega_{2,p+2}(t) & \cdots & \Omega_{2,p+N_c-2}(t) \\ \vdots & \vdots & \ddots & \vdots \\ \Omega_{V,p}(t) & \Omega_{V,p+2}(t) & \cdots & \Omega_{V,p+N_c-2}(t) \end{pmatrix}, \quad (1)$$

where V denotes the total number of symbols in each radar waveform, transmitted over L TDD downlink subframes. Therefore, L downlink subframes are combined to obtain a radar waveform during the radar processing, as in [25]. Considering that N_{sym} symbols are transmitted in each downlink subframe, the number of symbols processed for each radar waveform is $V = L \times N_{sym}$. Accordingly, each radar

processing involves a duration of $T_{rad} = L \times \Delta t$. Moreover, the first antenna (i.e. $p = 1$) transmits on the odd-numbered subcarriers (i.e. $n \in \{1, 3, \ldots, N_c - 1\}$), whereas the second antenna transmits on the even-numbered subcarriers (i.e. $n \in \{2, 4, \ldots, N_c\}$). The rows of this matrix denote the OFDM symbols and each columns denote the symbols transmitted on each subcarrier. This subcarrier allocation ensures that each antenna transmits orthogonal signals since only one antenna is active in each subcarrier while the entire spectrum is occupied by the radar in an interleaved way. Consequently, the transmitted waveform matrix by the radar is given by

$$\mathbf{S}_{rad}(t) = \left(\mathbf{S}_1(t) \,|||\, \mathbf{S}_2(t)\right), \tag{2}$$

where $|||$ indicates the interleaving of two antenna waveform matrices along the frequency axis[2]. Unlike conventional phased array radars, a MIMO radar transmitter does not usually perform beamforming; instead, it omnidirectionally emits orthogonal probing waveforms [26], and its receiver performs direction of arrival (DoA) estimation in addition to the range and velocity estimations to identify the targets.

B. Antenna Direct-Coupling Model

Since the radar receive antennas operate at the same time as the radar and communication transmit antennas during downlink, the direct-coupling between the antennas needs to be considered while modeling the received radar returns from the targets. The radar receive antennas must be carefully isolated from the radar transmit and communication antennas so as not to be directly affected by the transmitted signals. This level of isolation can be achieved by an appropriate antenna array design [27], and isolating the transmit antenna [28]. For instance, -70 dB isolation is achieved in [28]. Moreover, the distance between the transmit and receive radar antennas can be increased, or analog (RF) interference and digital (baseband) interference cancellation techniques can be employed to alleviate the direct-coupling between the transmit and receive antennas [25]. Note that the direct-coupling between the radar receive antennas and other antennas is not unique to the proposed system model, but rather a problem that exist in all continuous-wave radars. In the case of having a large number of antennas, it is not practical to implement RF interference cancellation since it would require analog circuitry between each RF chain. Therefore, a baseband digital direct-coupling cancellation is employed as illustrated in Fig. 2. Considering that the antenna array is fixed, the direct-coupling between the elements can be assumed deterministic compared to the very short coherence time of the network. Let $\mathbf{C}_c \in \mathbb{C}^{M\times Q}$ and $\mathbf{C}_r \in \mathbb{C}^{P\times Q}$ denote the direct-coupling matrices between Q radar receive antennas and M communication antennas, and P radar transmit antennas, respectively. The direct-coupling between the mth and the qth elements, i.e. $c_{mq} \in \mathbf{C}_c$ or $c_{pq} \in \mathbf{C}_r$, is modeled as $c_{mq} = \Lambda_{mq} e^{(-2\pi j d_{mq}/\lambda)}$ [29], where Λ_{mq} denotes the channel gain of the direct-coupling, i.e. $\Lambda_{mq}[\text{dB}] = -70$ dB [28], and d_{mq} denotes the distance between the two antenna elements. Such direct-coupling matrices can be estimated [30] and their impact on the received radar returns can be removed while processing the received baseband signals [25]. In this study, the radar is calibrated, to eliminate self-interference, such that the direct-coupling matrices are estimated then their products with the transmitted symbols are canceled from the received radar signals.

[2]It is possible to employ more than two antennas for the radar with the same subcarrier allocation pattern. For more information see [22], [24].

C. Communication and Radar Channels and CSI Estimation

The proposed precoder utilizes the CSI of the UEs, hence, it is necessary to explain the CSI estimation stage along with the communication and radar channel models. In the CSI estimation stage, the channel information between the UEs and the communication and radar antennas can be acquired by exploiting orthogonal pilot symbols transmitted by the UEs as both systems employ OFDM waveforms. Accordingly, the estimated channel matrix between K UEs and the communication antenna array, $\hat{\mathbf{H}}_{com} \in \mathbb{C}^{M\times K}$, along with the estimated channel between the radar transmit antennas and K UEs, $\hat{\mathbf{H}}_{rad} \in \mathbb{C}^{P\times K}$, can be effectively acquired. Note that these estimated channel matrices are only valid during the coherence time τ, hence CSI estimation must be regularly performed at the beginning of each TDD frame. The channels between the BS and the UEs are assumed to be non-line-of-sight (NLOS). Particularly, they can be modeled as Rayleigh fading corresponding to independent and identically distributed (i.i.d.) complex-valued channel matrices as $\mathbf{H}_{com} \in \mathbb{C}^{M\times K}$ consisting of $h_{m,k} \sim \mathcal{CN}(0, \sigma_k^2)$ and $\mathbf{H}_{rad} \in \mathbb{C}^{P\times K}$ consisting of $h_{p,k} \sim \mathcal{CN}(0, \sigma_k^2)$ independent complex random variables, where the path-loss of the kth UE is given by $\mathbb{E}\left[|h_{m,k}|^2\right] = \mathbb{E}\left[|h_{p,k}|^2\right] = \sigma_k^2$. For the sake of simplicity, σ_k^2 is assumed to be the same for all UEs.

Channel estimation using orthogonal pilot sequences can be performed by linear estimators such as the least-squares (LS) or the minimum mean square error (MMSE) estimators. However, pilot contamination, channel correlation, RF chain mismatch (i.e. non-symmetric hardware components), or additive white Gaussian noise (AWGN) may cause imperfect CSI estimation [31]. Accordingly, instead of considering a specific channel estimator, a generic imperfect CSI model is adopted here [32], [33] in which the estimated channel matrices are

$$\hat{\mathbf{H}}_{com} = \sqrt{1-\xi}\mathbf{H}_{com} + \mathbf{E}_{com}, \tag{3}$$

and

$$\hat{\mathbf{H}}_{rad} = \sqrt{1-\xi}\mathbf{H}_{rad} + \mathbf{E}_{rad}, \tag{4}$$

where $\mathbf{E}_{com} \in \mathbb{C}^{M\times K}$ and $\mathbf{E}_{rad} \in \mathbb{C}^{P\times K}$ denote the corresponding error matrices consisting of complex Gaussian random values given by $e_{m,k} \sim \mathcal{CN}\left(0, \sigma_E^2\right)$ with 0 mean and variance $\sigma_E^2 = \xi\sigma_k^2$ and ξ is the error coefficient. Moreover, these error matrices are independent of $\mathbf{H}_{com}$ and $\mathbf{H}_{rad}$. The total communication transmit power output is denoted by p_{com} and the total radar transmit power output is denoted by p_{rad}. As imperfect CSI is mainly caused by the signal-to-noise ratio (SNR), the error coefficient is modeled as $\xi = z\rho^{-a}$, where $\rho = p_{com}\sigma_k^2/\sigma_n^2$ denotes the SNR of each UE, and σ_n^2 is the noise variance, while z and a are

used to produce error matrices that are a function of SNR. Note that scaling down the channel matrices with $\sqrt{1-\xi}$ ensures that the estimated channel matrices have the same variance as the real channel matrices such that $\mathbb{E}\left[\left|h_{m,k}\right|^2\right] = \mathbb{E}\left[\left|\hat{h}_{m,k}\right|^2\right] = \mathbb{E}\left[\left|\sqrt{1-\xi}h_{m,k}\right|^2\right] + \mathbb{E}\left[\left|e_{m,k}\right|^2\right]$, where $\hat{h}_{m,k}$, $h_{m,k}$ and $e_{m,k}$ denote each element of matrices $\hat{\mathbf{H}}_{com}$, $\mathbf{H}_{com}$, $\mathbf{E}_{com}$, respectively. A similar notation is also followed for the radar-UE interference channel matrix $\mathbf{H}_{rad}$.

III. MIMO Precoder with Radar Interference

The downlink massive MIMO signals are precoded to constructively interfere with radar signals by exploiting the channel diversity at the UEs. Although the BS has only the channel knowledge of the UEs and no prior knowledge of the targets, it can beamform the communication symbols towards the desired UEs while striving to utilize the radar interference on them. On the other hand, the targets are to be substantially illuminated by the radar waveform since the communication signals will destructively interfere with each other in other directions. Since the channel between the radar transmit antennas and the UEs can be estimated along with the communication CSI using the same hardware, the phase and amplitude of the radar interference at the UEs are predictable [34]. Consequently, we introduce a low-complexity precoder which exploits this predictable radar interference and endeavors to utilize it into the desired symbols. This method does not require a particular radar beamforming, and thus, it provides greater flexibility to the radar such that omnidirectional or directional radar waveforms can be emitted. A power ratio between the radar and communication power outputs is defined as $\Psi = p_{rad}/p_{com}$. It is worth noting that communication signals are transmitted by M (e.g. 50 or more) antennas and the radar signals are assumed to be transmitted by only a few antennas (e.g. $P = 2$). Hence, this corresponds to the power per radar antenna being much higher than the power per communication antenna even if the total transmit powers are the same i.e. $\Psi = 1$. Only one OFDM subchannel is considered to explain the proposed precoder as this process can be performed concurrently in all subcarriers.

Although, the proposed RadCom architecture can be used with other precoder techniques e.g. maximum-likelihood (ML) precoder or minimum-mean-squared-error (MMSE) precoder, the zero-forcing (ZF) precoder is considered in this study because of its near-optimum performance with relatively less-complexity. The ZF precoder, denoted by $\mathbf{W}_{ZF} \in \mathbb{C}^{K\times M}$, is fundamentally the pseudoinverse of the estimated communication channel matrix $\hat{\mathbf{H}}_{com}$ as given by

$$\mathbf{W}_{ZF} = \left(\hat{\mathbf{H}}_{com}^H \hat{\mathbf{H}}_{com}\right)^{-1} \hat{\mathbf{H}}_{com}^H. \tag{5}$$

In a single-cell massive MIMO RadCom system, the received baseband signal vector $\widetilde{\mathbf{x}} \in \mathbb{C}^{K\times 1}$ by K UEs on each subcarrier during one symbol duration is given by

$$\widetilde{\mathbf{x}} = \mathbf{H}_{com}^H \mathbf{y} + \mathbf{h}_{rad}^H \sqrt{p_{rad}} s_p + \mathbf{n}, \tag{6}$$

where $\mathbf{n} \in \mathbb{C}^{K\times 1}$denotes the zero-mean complex circular symmetric Gaussian noise vector with covariance matrix $\mathbb{E}\left[\mathbf{n}\mathbf{n}^H\right] = \sigma_n^2 \mathbb{I}$, where $\mathbb{I}$ is the $K \times K$ identity matrix. Also, $\mathbf{y} \in \mathbb{C}^{M\times 1}$ denotes the precoded communication symbols transmitted by M communication antennas, as given by

$$\mathbf{y} = \sqrt{p_{com}} \alpha_{ZF} \mathbf{W}_{ZF}^H \mathbf{x}, \tag{7}$$

vector $\mathbf{x} \in \mathbb{C}^{K\times 1} = [x_1\ x_2\ ...\ x_K]^T$ contains the data symbols intended to be transmitted by the BS to K UEs. Only one radar transmit antenna is active on each subcarrier due to the interleaved OFDM radar waveform as explained before, and hence, $\mathbf{h}_{rad} \in \mathbb{C}^{1\times K}$ denotes the channel between K UEs and the active radar antenna on this subcarrier. Moreover, s_p denotes the transmitted radar symbol by the active radar transmit antenna on this subcarrier. Also, α_{ZF} is the power coefficient to satisfy the power condition of the transmitted communication signals by the entire antenna array as $\mathbb{E}\left[\left\|\alpha_{ZF}\mathbf{W}_{ZF}^H\mathbf{x}\right\|^2\right] = 1$, and thus,

$$\alpha_{ZF} = 1/\sqrt{\mathbb{E}\left[tr\left(\mathbf{W}_{ZF}\mathbf{W}_{ZF}^H\right)\right]} = \sqrt{\frac{M-K}{K}}, \tag{8}$$

can be set without considering radar interference [35]. To maximize the downlink communication data rate, the interference at the UEs from the radar needs to be minimized as

$$\min_{s_p,\, p_{rad}} \quad \left\|\sqrt{p_{rad}}\mathbf{h}_{rad}^H s_p\right\|^2 \tag{9}$$

$$s.t. \quad \frac{p_{rad}}{p_{com}} \geq \Psi, \tag{10}$$

$$\frac{\|\mathbf{S}_{rad}\|_F^2}{VN_c} = 1, \tag{11}$$

$$\left\|\alpha_{ZF}\mathbf{W}_{ZF}^H\mathbf{x}\right\|^2 = 1, \tag{12}$$

where (10) is the power ratio constraint between the radar and the communication output powers, (11) ensures that the transmitted radar waveform given by (1) during one TDD frame through all subcarriers has unit average power and $s_p \in \mathbf{S}_{rad}$. Finally, the last constraint (12) limits the power transmitted by the antenna array. Due to the power constraint (10), it is not possible to decrease the radar output power as it would proportionally degrade the radar detection performance. Thus, instead of attempting to minimize the radar output power, creating constructive interference with the incident radar signals at the UEs is pursued. Considering the communication signals transmitted and the radar waveform emitted by the BS, i.e. substituting (7) into (6), the received baseband symbol vector $\widetilde{\mathbf{x}} = [\widetilde{x}_1\ \widetilde{x}_2\ ...\ \widetilde{x}_K]^T$ by K UEs will be

$$\widetilde{\mathbf{x}} = \sqrt{p_{com}}\mathbf{H}_{com}^H \alpha_{ZF} \mathbf{W}_{ZF}^H \mathbf{x} + \underbrace{\mathbf{h}_{rad}^H \sqrt{p_{rad}} s_p}_{\boldsymbol{\Upsilon}_{\mathbf{rad}}} + \mathbf{n}. \tag{13}$$

Let us assume that the interference caused by the radar waveform (Υ_{rad}) can be eliminated by vector $\boldsymbol{\Theta} \in \mathbb{C}^{M\times 1}$, which is transmitted within the precoded communication symbols as

$$\widetilde{\mathbf{x}} = \sqrt{p_{com}}\mathbf{H}_{com}^H \left(\alpha_{ZF}\mathbf{W}_{ZF}^H\mathbf{x} - \frac{\boldsymbol{\Theta}}{\sqrt{p_{com}}}\right) + \sqrt{p_{rad}}\mathbf{h}_{\mathbf{rad}}^H s_p, \tag{14}$$

where the noise vector is neglected for the sake of simplicity. After rearranging this equation, $\widetilde{\mathbf{x}}$ is obtained as

$$\widetilde{\mathbf{x}} = \underbrace{\sqrt{p_{com}}\mathbf{H}_{com}^{H}\alpha_{ZF}\mathbf{W}_{ZF}^{H}\mathbf{x}}_{\hat{\mathbf{x}}} - \mathbf{H}_{com}^{H}\boldsymbol{\Theta} + \sqrt{p_{rad}}\mathbf{h}_{rad}^{H}s_p, \tag{15}$$

where the first term, indicated by $\hat{\mathbf{x}}$, denotes the symbol vector desired to be received at the UEs. Hence, the second and the third terms must cancel out each other to eliminate the radar interference. This results in

$$\boldsymbol{\Theta} = \left(\mathbf{H}_{com}^{H}\right)^{-1}\left(\sqrt{p_{rad}}\mathbf{h}_{rad}^{H}s_p\right), \tag{16}$$

where $\left(\mathbf{H}_{com}^{H}\right)^{-1}$ denotes the inverse of $\mathbf{H}_{com}^{H}$, and the pseudoinverse matrix $\mathbf{H}_{com}^{\dagger}$ (Moore–Penrose inverse) of the channel is used instead of $\left(\mathbf{H}_{com}^{H}\right)^{-1}$, as it is the same as the ZF receiver and can be obtained based on the estimated communication channel matrix $\hat{\mathbf{H}}_{com}$. Accordingly, vector $\boldsymbol{\Theta}$ shall be equal to

$$\begin{aligned}\boldsymbol{\Theta} &= \sqrt{p_{rad}}\mathbf{W}_{ZF}^{H}\hat{\mathbf{h}}_{rad}^{H}s_p \\ &= \sqrt{p_{rad}}\left[\left(\hat{\mathbf{H}}_{com}^{H}\hat{\mathbf{H}}_{com}\right)^{-\mathbf{1}}\hat{\mathbf{H}}_{com}^{H}\right]^{H}\hat{\mathbf{h}}_{rad}^{H}s_p.\end{aligned} \tag{17}$$

This operation requires only the estimated channels $\hat{\mathbf{H}}_{com}$ and $\hat{\mathbf{h}}_{rad}$ which can be conveniently acquired during uplink CSI estimation as explained before. Hence, the transmitted precoded signal vector is given by

$$\mathbf{y} = \underbrace{\sqrt{p_{com}}\left(\alpha_{ZF}\mathbf{W}_{ZF}^{H}\mathbf{x}\right)}_{useful\ signal} - \underbrace{\sqrt{p_{rad}}\mathbf{W}_{ZF}^{H}\hat{\mathbf{h}}_{rad}^{H}s_p}_{radar\ IC}, \tag{18}$$

where the first term consists of the symbols to be transmitted to the UEs while the second term is the radar interference cancellation signal. Substituting $p_{rad} = \Psi p_{com}$, and given that $\mathbf{H}_{com}$, $\mathbf{h}_{rad}$, $\mathbf{x}$ and s_p are random complex matrices, vectors or scalars and they are independent of each other, this precoder can be simplified as

$$\mathbf{y} = \sqrt{p_{com}}\mathbf{W}_{ZF}^{H}\left(\alpha_{ZF}\mathbf{x} - \sqrt{\Psi}\hat{\mathbf{h}}_{rad}^{H}s_p\right), \tag{19}$$

which requires only one pseudoinverse computation, and hence, its complexity is comparable to the ZF precoder. Although the sign of the radar interference cancellation term ($\sqrt{\Psi}\hat{\mathbf{h}}_{rad}^{H}s_p$) is negative, transmitting (19) instead of (7) requires an increase in the power transmitted (i.e. $\|\mathbf{y}\|^2$) by the communication array, since $\alpha_{ZF}\mathbf{x}$ and $\sqrt{\Psi}\hat{\mathbf{h}}_{rad}^{H}s_p$ are mutually independent and random complex vectors. Therefore, this precoder may cause an increase in the transmitted output power by the communication array, if α_{ZF} is kept constant. The total power transmitted by the array is expressed by

$$p_u = \left\|\mathbf{W}_{ZF}^{H}\left(\alpha_{ZF}\mathbf{x} - \sqrt{\Psi}\hat{\mathbf{h}}_{rad}^{H}s_p\right)\right\|^2, \tag{20}$$

and this can be decomposed into the useful symbol power given by

$$p_{sym} = \left\|\alpha_{ZF}\mathbf{W}_{ZF}^{H}\mathbf{x}\right\|^2, \tag{21}$$

and the power used for radar interference cancellation operation given by

$$p_{ric} = \left\|\mathbf{W}_{ZF}^{H}\sqrt{\Psi}\hat{\mathbf{h}}_{rad}^{H}s_p\right\|^2. \tag{22}$$

Accordingly, the total symbol power can be expressed by $p_u = p_{sym} + p_{ric}$ as the communication and radar signals are random complex values and independent of each other. Hereby, we introduce an adaptive α_{ZF} calculation to satisfy the unit power condition by taking into account the power required to eliminate the radar interference. Accordingly, α_{ZF} must be updated as

$$\alpha_{ZF} = \sqrt{\frac{M-K}{K}\left(1 - \Psi\left\|\mathbf{W}_{ZF}^{H}\hat{\mathbf{h}}_{rad}^{H}\right\|^2\right)}, \tag{23}$$

which decreases as the radar output power increases to satisfy the power output constraint for the antenna array. This adaptive α_{ZF} computation requires only the knowledge of the precoder matrix and the estimated channel matrices, and thus, can be performed within the CSI estimation stage at the beginning of each TDD frame.

IV. Optimum OFDM Radar Waveform Design

Unlike correlation based radar, the symbol-based OFDM radar processing employed here, the estimation performance of the radar is independent of the transmitted data in the waveform, [22], [36]. The optimum radar waveform (ORWF) to maximize the channel capacity can be designed by minimizing the distance between the communication symbols and the radar interference received at the UEs. By doing so, the interfering radar signals at the UEs will be closer to the indented symbols transmitted to the UEs and hence less power can be used to move this interference to the indented symbols' detection area.

A. Optimum Radar Waveform Design

The optimum radar waveform design problem is expressed as follows

$$s_p = \underset{s_p}{\operatorname{argmin}} \quad \left\|\alpha_{ZF}\mathbf{x} - \sqrt{\Psi}\hat{\mathbf{h}}_{rad}^{H}s_p\right\|^2 \tag{24}$$

$$s.t. \qquad \frac{\|\mathbf{S}_p\|_F^2}{VN_c} = 1, \tag{25}$$

$$\left\|\alpha_{ZF}\mathbf{W}_{ZF}^{H}\mathbf{x}\right\|^2 = 1. \tag{26}$$

If a QAM scheme is used, then solving this optimization problem could be computationally-intensive because of constraint (25) which considers the entire radar waveform matrix. However, a constant modulus modulation scheme, such as phase shift keying (PSK), can be used. Employing PSK with R constellation size (e.g. $R = 4$ for QPSK or $R = 16$ for 16-PSK) reduces this problem to a search problem which can be solved in R steps, since constraint (25) will be inherently satisfied by phase modulation schemes, and the unit power constraint of the communication symbols given by (26) can be satisfied by further adjusting α_{ZF}. This optimum radar symbol selection reduces the power required for radar signal cancellation, p_{ric}, resulting in a larger part of the transmitted

Algorithm 1 Proposed Precoder for RadCom

1 : **Input :** s_p, $\mathbf{x}$, p_{com}, and p_{rad}.
2 : FOR each TDD frame
3 : FOR each pilot symbol
4 : UEs transmit orthogonal pilot symbols ;
5 : BS estimates channel matrices : $\hat{\mathbf{H}}_{com}$ and $\hat{\mathbf{H}}_{rad}$;
6 : END FOR
7 : Compute the precoder matrix by (19) ;
8 : Satisfy power constraint by (23) ;
9 : Determine the optimum radar waveform by (24) ;
10 : Calculate β_{ZF} by (27) ;
11 : Transmit precoded signals and radar waveforms ;
12 : END FOR
13 : **Output :** $\mathbf{y}$ and s_p.

power by the array to be allocated for the communication. After selecting the optimum radar symbols, they will be dependent on the transmitted communication symbols and estimated channels, hence α_{ZF} given by (23) may not satisfy the unit power constraint. In this case, to satisfy the transmit power constraint, a scaling factor β_{ZF} is introduced, which is approximated by

$$\beta_{ZF} \approx \mathbb{E}\left[\left\|\alpha_{ZF}\mathbf{W}_{ZF}^{H}\mathbf{x} - \sqrt{\Psi}\mathbf{W}_{ZF}^{H}\hat{\mathbf{h}}_{rad}^{H}s_p\right\|^2\right]^{-1/2}, \quad (27)$$

which yields $\beta_{ZF} > 1$. Then the transmitted signal vector with the optimum radar waveform can be given by

$$\mathbf{y} = p_{com}\beta_{ZF}\alpha_{ZF}\mathbf{W}_{ZF}^{H}\mathbf{x} - \mathbf{W}_{ZF}^{H}\sqrt{\Psi}\hat{\mathbf{h}}_{rad}^{H}s_p, \quad (28)$$

where the radar waveform is optimized by (24) depending on the communication symbols and the channel conditions. Algorithm 1 summarizes the mechanism of the proposed precoder including CSI estimation and downlink transmission.

B. Computational Complexity of the Proposed Precoder

The computational complexity of the proposed method in terms of floating-point operations (FLOPs) is analyzed here. The complexity of each operation, e.g. multiplication, summation, square-root, is assumed to be $\mathcal{O}(1)$, and matrix transposes require no FLOPs [37]. The complexity of calculating the ZF precoder matrix given by (5) requires one matrix-matrix multiplication, (i.e. $\mathcal{O}\left(2K^2M - K^2\right)$), one matrix inversion, (i.e. $\mathcal{O}\left(K^3 + K^2\right)$) [38], another matrix-matrix multiplication, (i.e. $\mathcal{O}\left(2K^2M - MK\right)$), and hence, its overall complexity is $\mathcal{O}\left(K^3 + 4K^2M - MK\right)$. Table I presents the complexity of the equations used in the proposed RadCom precoder. Note that the computed pseudoinverse of the channel matrix can be used in (19), (23), (24) and (27), and thus, it should be computed only once and its complexity is included only in (19). Hence, the overall complexity of Algorithm 1 without ORWF is then given by $\mathcal{O}\left(K^3 + 4K^2M + 5MK + 2M + 4K\right)$, and its complexity with ORWF is given by $\mathcal{O}\left(K^3 + 4K^2M + 7MK + 6RK + 5M + 4K + R\right)$.
The complexity of ZF is $\mathcal{O}\left(K^3 + 4K^2M + MK + 2M\right)$. It can be observed that the proposed precoder has a similar complexity to ZF, since the main computational complexity is caused by computing the pseudoinverse of the channel matrix. Computing the optimum radar waveform might introduce extra computational complexity depending on the constellation size R of the PSK modulation used in the radar waveform; however, it is still relatively low compared to the matrix inversion complexity. Lastly, the extra complexity caused by the ORWF design can be reduced by using a QPSK radar waveform, instead of high-order modulated waveforms. This will decrease the complexity of the ORWF; however, at the cost of decreasing the network sum-capacity.

Table I
COMPLEXITY OF THE EQUATIONS USED IN ALGORITHM 1.

Equation	Complexity [FLOPs]
(19)	$K^3 + 4K^2M + 3MK + 4K$
(23)	$2MK + 2M$
(24)	$6RK + R$
(27)	$2MK + 3M$

V. CAPACITY ANALYSIS

This section analyses the capacity of the proposed precoder for the perfect and imperfect CSI cases. The transmitted communication and radar symbol vectors have unit average power i.e. $\mathbb{E}\left[|x_k|^2\right] = 1\ \forall k$ and $\mathbb{E}\left[|s_p|^2\right] = 1$ due to the use of PSK modulation for the radar waveform. Therefore, these two parameters are dropped from the power equations. Furthermore, the channel gain of the UEs is normalized as $\mathbb{E}\left[|h_{m,k}|^2\right] = 1$ and $\mathbb{E}\left[|h_{p,k}|^2\right] = 1$, and hence, $\mathbb{E}\left[|e_{m,k}|^2\right] = \xi$ and $\mathbb{E}\left[|e_{p,k}|^2\right] = \xi$. The variance of the AWGN sample n_k is given by $\mathbb{E}\left[|n_k|^2\right] = \sigma_n^2$ at the kth UE.

A. Perfect CSI Case

When the BS perfectly estimates CSI, the received signal of the kth UE can be given by

$$\hat{x}_k = \mathbf{h}_{com,k}^{H}\left(\sqrt{p_{com}}\beta_{ZF}\alpha_{ZF}\mathbf{w}_k^{H}x_k - \sqrt{p_{rad}}\mathbf{w}_k^{H}\hat{h}_{rad,k}^{*}s_p\right) + \sum_{i=1,i\neq k}^{K}\mathbf{h}_{com,k}^{H}\left(\sqrt{p_{com}}\beta_{ZF}\alpha_{ZF}\mathbf{w}_i^{H}x_i - \sqrt{p_{rad}}\mathbf{w}_i^{H}\hat{h}_{rad,i}^{*}s_p\right) + \sqrt{p_{rad}}h_{rad,k}^{*}s_p + n_k, \quad (29)$$

where $\mathbf{h}_{com,k} \in \mathbb{C}^{M\times 1}$ denotes the channel vector between the kth UE and the antenna array, $\mathbf{w}_k^{H} \in \mathbb{C}^{1\times M}$ denotes the kth row of the ZF precoder corresponding to the kth UE, and $h_{rad,k}$ denotes the interference channel between the kth UE and the active radar antenna on that subcarrier. The first term consists of the symbols to be transmitted to the kth UE and the signal to cancel the predicted radar interference at that UE. The second term refers to the interference from other UEs and the third term is the interference induced by the radar. This can be rearranged as

$$\hat{x}_k = \underbrace{\sqrt{p_{com}}\beta_{ZF}\alpha_{ZF}\mathbf{h}_{com,k}^H\mathbf{w}_k^H x_k}_{\Upsilon_k} + \underbrace{\sqrt{p_{com}}\sum_{i=1,i\neq k}^{K}\mathbf{h}_{com,k}^H\mathbf{w}_i^H\left(\beta_{ZF}\alpha_{ZF}x_i - \sqrt{\Psi}\hat{h}_{rad,i}^* s_p\right)}_{\Upsilon_{iu}} + \underbrace{\sqrt{p_{rad}}s_p\left(h_{rad,k}^* s_p - \mathbf{h}_{com,k}^H\mathbf{w}_k^H\hat{h}_{rad,k}^*\right)}_{\Upsilon_{rad}} + n_k, \quad (30)$$

where Υ_{iu} and Υ_{rad} express the inter-user interference and the residual radar interference after the radar interference cancellation, respectively. The average signal-to-interference-plus-noise ratio ($SINR_k$) for the kth UE is calculated by

$$SINR_k = \frac{\mathbb{E}\left[\left|\Upsilon_k\right|^2\right]}{\mathbb{E}\left[\left|\Upsilon_{iu}\right|^2\right] + \mathbb{E}\left[\left|\Upsilon_{rad}\right|^2\right] + \sigma_n^2}. \quad (31)$$

When the BS perfectly estimates both channel matrices, $\hat{\mathbf{h}}_{com,i} = \mathbf{h}_{com,i}$ and $\hat{h}_{rad,i} = h_{rad,i}$ will be obtained. As the channel coefficients are assumed to be i.i.d., then $\mathbb{E}\left[\left|\mathbf{h}_{com,k}^H\mathbf{w}_k^H\right|\right] = \mathbb{E}\left[\left|\hat{\mathbf{h}}_{com,k}^H\mathbf{w}_k^H\right|\right] \cong 1$ and $\mathbb{E}\left[\left|\mathbf{h}_{com,k}^H\mathbf{w}_i^H\right|\right] = \mathbb{E}\left[\left|\hat{\mathbf{h}}_{com,k}^H\mathbf{w}_i^H\right|\right] \cong 0$ can be given if $i \neq k$, and the number of BS antennas is sufficiently large (i.e. $M_c \gg K$). Hence, the average received useful signal power is calculated as

$$\begin{aligned}\mathbb{E}\left[\left|\Upsilon_k\right|^2\right] &= p_{com}\beta_{ZF}^2\alpha_{ZF}^2\mathbb{E}\left[\left|\mathbf{h}_{com,k}^H\mathbf{w}_k^H\right|^2\right] \\ &= p_{com}\beta_{ZF}^2\alpha_{ZF}^2, \end{aligned} \quad (32)$$

and the power of the interference from the symbols transmitted to the other UEs will be

$$\begin{aligned}\mathbb{E}\left[\left|\Upsilon_{iu}\right|^2\right] &= p_{com}\beta_{ZF}^2\alpha_{ZF}^2\sum_{i=1,i\neq k}^{K}\mathbb{E}\left[\left|\mathbf{h}_{com,k}^H\mathbf{w}_i^H\right|^2\right] \\ &+ p_{rad}\sum_{i=1,i\neq k}^{K}\mathbb{E}\left[\left|-\mathbf{h}_{com,k}^H\mathbf{w}_i^H\hat{h}_{rad,i}^*\right|^2\right] \cong 0. \end{aligned} \quad (33)$$

The power of the residual radar interference after interference cancellation can be given by

$$\mathbb{E}\left[\left|\Upsilon_{rad}\right|^2\right] = p_{rad}\mathbb{E}\left[\left|h_{rad,k}^* s_p - \mathbf{h}_{com,k}^H\mathbf{w}_k^H\hat{h}_{rad,k}^* s_p\right|^2\right] \cong 0. \quad (34)$$

Consequently, the downlink achievable capacity of the kth UE with perfect CSI is given by

$$\begin{aligned}C_k &= \log_2\left(1 + SINR_k\right) \\ &\cong \log_2\left(1 + \frac{\beta_{ZF}^2\alpha_{ZF}^2 p_{com}}{\sigma_n^2}\right), \end{aligned} \quad (35)$$

where α_{ZF} is given by (23) and β_{ZF} is given by 27. Finally, the achievable downlink sum-capacity of the entire network can be computed by $C_{sum} = \sum_{k=1}^{K} C_k$. As a performance benchmark, the lower bound of the ZF capacity under favorable channel conditions is used, as [35]

$$C_{ZF} \geq \log_2\left(1 + \frac{p_{com}\left(M-K\right)}{K\sigma_n^2}\right). \quad (36)$$

B. Imperfect CSI Case

If there is a CSI error such that $\xi \neq 0$ with regards to (3) and (4), then the real channel vectors are given by

$$\mathbf{h}_{com,k} = \frac{\hat{\mathbf{h}}_{com,k} - \mathbf{e}_{com,k}}{\sqrt{1-\xi}}, \text{ and } \mathbf{h}_{rad,k} = \frac{\hat{\mathbf{h}}_{rad,k} - \mathbf{e}_{rad,k}}{\sqrt{1-\xi}}, \quad (37)$$

respectively, where $\mathbf{e}_{com,k} \in \mathbb{C}^{M\times 1}$ and $\mathbf{e}_{rad,k} \in \mathbb{C}^{P\times 1}$ are the corresponding error vectors for the kth UE's estimated CSI. The channel vectors can be substituted with the imperfectly estimated CSI vectors in (19) to obtain the useful signal vector Υ_k as

$$\Upsilon_k = \sqrt{p_{com}}\beta_{ZF}\alpha_{ZF}\frac{\left(\hat{\mathbf{h}}_{com,k}^H\mathbf{w}_k^H - \mathbf{e}_{com,k}^H\mathbf{w}_k^H\right)}{\sqrt{1-\xi}}. \quad (38)$$

Thus, the average power of the useful signal can be given by

$$\begin{aligned}\mathbb{E}\left[\left|\Upsilon_k\right|^2\right] &= \frac{p_{com}\beta_{ZF}^2\alpha_{ZF}^2}{1-\xi}\mathbb{E}\left[\left|\hat{\mathbf{h}}_{com,k}^H\mathbf{w}_k^H - \mathbf{e}_{com,k}^H\mathbf{w}_k^H\right|^2\right] \\ &= \frac{p_{com}\beta_{ZF}^2\alpha_{ZF}^2}{1-\xi}\Bigg(\mathbb{E}\left[\left|\hat{\mathbf{h}}_{com,k}^H\mathbf{w}_k^H\right|^2\right] \\ &- 2\mathbb{E}\left[\left|\hat{\mathbf{h}}_{com,k}^H\mathbf{w}_k^H\right|\right]\mathbb{E}\left[\left|\mathbf{e}_{com,k}^H\mathbf{w}_k^H\right|\right] \\ &+ \mathbb{E}\left[\left|\left(\mathbf{e}_{com,k}^H\mathbf{w}_k^H\right)^2\right|\right]\Bigg), \end{aligned} \quad (39)$$

where $\mathbb{E}\left[\left|\mathbf{e}_{com,k}^H\mathbf{w}_k^H\right|\right] = \xi$, and

$$\mathbb{E}\left[\left|\mathbf{e}_{com,k}^H\mathbf{w}_k^H\right|^2\right] \approx \xi^2 + \frac{\xi}{M-K}. \quad (40)$$

Proof: See Appendix. ∎

Consequently, the analytical expression of the useful signal power for the kth UE is obtained as

$$\begin{aligned}\mathbb{E}\left[\left|\Upsilon_k\right|^2\right] &\approx \frac{p_{com}\beta_{ZF}^2\alpha_{ZF}^2}{1-\xi}\left(1 - 2\xi + \xi^2 + \frac{\xi}{M-K}\right) \\ &\approx \frac{p_{com}\beta_{ZF}^2\alpha_{ZF}^2}{1-\xi}\left(\left(1-\xi\right)^2 + \frac{\xi}{M-K}\right) \\ &\approx p_{com}\beta_{ZF}^2\alpha_{ZF}^2\left(1 - \xi + \frac{\xi}{\left(M-K\right)\left(1-\xi\right)}\right). \end{aligned} \quad (41)$$

Including channel estimation errors in (33), the interference from other UEs can be given by

$$\Upsilon_{iu} = \sqrt{p_{com}}\sum_{i=1,i\neq k}^{K}\left[\frac{\hat{\mathbf{h}}_{com,k}^H\mathbf{w}_i^H - \mathbf{e}_{com,k}^H\mathbf{w}_i^H}{\sqrt{1-\xi}}\left(\beta_{ZF}\alpha_{ZF} - \sqrt{\Psi}\hat{h}_{rad,i}^*\right)\right], \quad (42)$$

and the power of this interference will be

$$\mathbb{E}\left[\left|\Upsilon_{iu}\right|^2\right] = \frac{p_{com}}{1-\xi}\sum_{i=1,i\neq k}^{K}\Big(\beta_{ZF}^2\alpha_{ZF}^2\mathbb{E}\left[\left|\mathbf{e}_{com,k}^H\mathbf{w}_i^H\right|^2\right] + \Psi\mathbb{E}\left[\left|\mathbf{e}_{com,k}^H\mathbf{w}_i^H\right|^2\right]\mathbb{E}\left[\left|\hat{h}_{rad,i}^*\right|^2\right]\Big)$$
$$= \frac{p_{com}}{1-\xi}\sum_{i=1,i\neq k}^{K}\mathbb{E}\left[\left|\mathbf{e}_{com,k}^H\mathbf{w}_i^H\right|^2\right]\left(\beta_{ZF}^2\alpha_{ZF}^2+\Psi\right), \quad (43)$$

where $\mathbb{E}\left[\left|\hat{h}_{rad,i}^*\right|^2\right] = 1$, and

$$\mathbb{E}\left[\left|\mathbf{e}_{com,k}^H\mathbf{w}_i^H\right|^2\right] \approx \frac{\xi}{M-K}. \quad (44)$$

Proof: See Appendix. ∎

Consequently, the power of the inter-user interference is

$$\mathbb{E}\left[\left|\Upsilon_{iu}\right|^2\right] \approx \frac{p_{com}\xi\left(\beta_{ZF}^2\alpha_{ZF}^2+\Psi\right)(K-1)}{(1-\xi)(M-K)}. \quad (45)$$

This equation shows that imperfect CSI may also cause an extra radar interference, and this is because, the signals sent to utilize the radar interference at other UEs can be received as an extra interference by the kth UE due to CSI estimation errors. The residual radar interference under imperfect CSI is found by substituting the CSI error vector into (34), yielding

$$\Upsilon_{rad} = \sqrt{\frac{p_{rad}}{1-\xi}}\times\Big[\left(\hat{h}_{rad,k}^* - e_{rad,k}^*\right) - \left(\hat{\mathbf{h}}_{com,k}^H\mathbf{w}_k^H - \mathbf{e}_{com,k}^H\mathbf{w}_k^H\right)\hat{h}_{rad,k}^*\Big]. \quad (46)$$

Furthermore, the power of this radar interference is given by

$$\mathbb{E}\left[\left|\Upsilon_{rad}\right|^2\right] = \frac{\Psi p_{com}}{1-\xi}\mathbb{E}\left[\left|-e_{rad,k}^* + \mathbf{e}_{com,k}^H\mathbf{w}_k^H\right|^2\right]$$
$$= \frac{\Psi p_{com}}{1-\xi}\Bigg(\mathbb{E}\left[\left|e_{rad,k}^*\right|^2\right] + \mathbb{E}\left[\left|\mathbf{e}_{com,k}^H\mathbf{w}_k^H\right|^2\right] - 2\mathbb{E}\left[\left|e_{rad,k}^*\right|\right]\mathbb{E}\left[\left|\mathbf{e}_{com,k}^H\mathbf{w}_k^H\right|\right]\Bigg), \quad (47)$$

where $\mathbb{E}\left[\left|e_{rad,k}^*\right|\right] \approx \sqrt{\xi}$, $\mathbb{E}\left[\left|\mathbf{e}_{com,k}^H\mathbf{w}_k^H\right|\right] = \xi$, and the analytical expression of the second term is given by (40), hence

$$\mathbb{E}\left[\left|\Upsilon_{rad}\right|^2\right] \approx \frac{\Psi p_{com}}{1-\xi}\left(\xi+\xi^2-2\xi\sqrt{\xi}+\frac{\xi}{M-K}\right). \quad (48)$$

Consequently, the SINR of the kth UE with imperfect CSI is derived as (49) shown at the top of the next page, and the channel capacity with imperfect CSI can be calculated by substituting $SINR_k^{imp}$ into (35).

VI. Radar Detection Performance

In addition to the capacity of the communication system, the accuracy of the target feature estimation is also an important performance metric that needs to be considered in RadCom systems. From the radar's perspective, communication signals would be perceived as interference degrading the accuracy of the detection. Assuming that U targets are present, the channel between the pth radar transmit antenna, targets and the qth radar receive antenna is calculated by element-wise division of the transmitted and received radar waveforms as [8]

$$\mathbf{G}_{qp}(n_p,\mu) = \frac{\mathbf{D}_q(n_p,\mu)+\mathbf{N}_q(n_p,\mu)}{\mathbf{S}_p(n_p,\mu)} = \sum_{u=1}^{U}\kappa_{p,u,q}e^{-j2\pi n_p\Delta f\Theta_u}e^{j2\pi f_{D,u}\mu t_o} + \frac{\mathbf{N}_q(n_p,\mu)}{\mathbf{S}_p(n_p,\mu)}, \quad (50)$$

where $\mathbf{D}_q(n_p,\mu)$ and $\mathbf{N}_q(n_p,\mu)$ denote the μth reflected symbol and the sum of the noise and interference at this symbol, respectively, received by the qth antenna in n_pth the subcarrier. $\mathbf{S}_p(n_p,\mu)$ denotes the (n_p,μ)th symbol of the radar waveform matrix transmitted by the pth radar transmit antenna. Moreover, $\kappa_{p,u,q}$ denotes the two-way channel gain given by

$$\kappa_{p,u,q} = \frac{\lambda\sqrt{G_{tx}G_{rx}\sigma_u}}{(4\pi)^{3/2}R_{u,p}R_{u,q}} \quad (51)$$

where $R_{u,p}$ and $R_{u,q}$ denote the distances between the radar transmit and receive antennas and the uth target, repectively. Moreover, $e^{-j2\pi n_p\Delta f\Theta_u}$ with $\Theta_u = (R_{u,p}+R_{u,q})/c_0$ denotes the phase shift that occurs due to the path length $(R_{u,p}+R_{u,q})$ along which electromagnetic waves travel. Also, c_0 denotes the speed of light, while G_{tx} and G_{rx} denote the gains of each transmit and receive antennas, respectively and σ_u is the radar cross-section (RCS) of the uth target. The second phase shift term, given by $e^{j2\pi f_{D,u}\mu t_o}$, includes velocity information of the targets. The Doppler shift caused by the target velocities is given by $f_{D,u} = 2v_u/\lambda$, where v_u denotes relative speed of the uth target. The noise, interference and direc-coupling matrix, $\mathbf{N}$, at the radar receive antennas is given by

$$\mathbf{N} = p_{com}\left(\Psi\mathbf{C}_r^H\mathbf{S}_{rad} + \mathbf{C}_c^H\mathbf{y} + \mathbf{G}_{com}^H\mathbf{y}\right) + \mathbf{w} + \mathbf{n}, \quad (52)$$

where the first three terms indicate the direct-coupling from radar transmit antennas, the direct-coupling from the communication antennas and the reflected communication signals from the targets. $\mathbf{S}_{rad} \in \mathbb{C}^{P\times V}$ denotes the transmitted symbols by radar transmit antennas. $\mathbf{G}_{com} \in \mathbb{C}^{Q\times M}$ denotes the interference channel between communication antennas, targets and the radar receive antennas and it is modeled similar to $\mathbf{G}_{qp}$. The clutter is denoted by $\mathbf{w}$ which includes other reflected signals from the surrounding area and it is distributed as $w \sim \mathcal{CN}\left(0,\sigma_w^2\right)$ and the AWGN noise $\mathbf{n}$ is distributed as $n \sim \mathcal{CN}\left(0,\sigma_n^2\right)$. As communication signals are precoded in order to be beamformed onto the UEs, the target is mostly illuminated by the omnidirectional radar waveform and it may receive some sidelobes from the communication signals. This inherently decreases the interference from the communication system to the radar.

A. Range and Velocity Estimation

To extract the range and velocity information of the targets, 2D Fourier transform can be applied through the frequency and time axes over the acquired channel data, $\mathbf{G}_{qp}$, for each radar transmit and receive antenna pair, respectively [22]. The range profile of the targets can be obtained by taking inverse fast Fourier transform (IFFT) of the obtained target channel

$$SINR_k^{imp} \approx \frac{p_{com}\beta_{ZF}^2\alpha_{ZF}^2\left(1-\xi+\frac{\xi}{(M-K)(1-\xi)}\right)}{\frac{p_{com}}{1-\xi}\left[\frac{\xi(K-1)}{M-K}\left(\beta_{ZF}^2\alpha_{ZF}^2+\Psi\right)+\Psi\left(\xi+\xi^2-2\xi\sqrt{\xi}+\frac{\xi}{M-K}\right)\right]+\sigma_n^2}. \quad (49)$$

matrix, $\mathbf{G}_{qp}$, through the subcarrier axis (n_p) for each radar transmit and receive antenna pair, and the velocity profile can be obtained by taking the FFT of the obtained matrix through the symbol axis (μ), given by [8], [22], [39]

$$\mathbf{D}_{qp} = \text{FFT}_{\mu}\left[\text{IFFT}_{n_p}\left[\mathbf{G}_{qp}\right]\right]. \quad (53)$$

Acquired range-velocity profiles ($\mathbf{D}_{qp} \in \mathbb{C}^{V\times N_c/P}$) will have a processing gain of $G_p = VN_c/P$ obtained by the FFT/IFFT operations, and hence, the SINR of the radar image is multiplied by G_p after the range-velocity processing.

B. Estimation of Direction of Arrivals (DoA)

Since the ULA is considered as the radar receive antenna array, only azimuth angles of the targets are estimated here, however, it is also possible to estimate the elevation angles by using a uniform rectangular array (URA). DoA estimation can be performed using different methods such as Fourier Beamforming, MUSIC or ESPRIT methods [22]. For the sake of simplicity, the Fourier Beamforming method is used in this study for DoA estimation. Assume that the range-velocity matrices are summed along the velocity axis such that $\mathbf{D}_{p,q}(n_p) = \sum_{\mu=1}^{V}\mathbf{D}_{p,q}(n_p,\mu)$, and thus, each row of these matrices can be rearranged as

$$\mathbf{D}(n_p) = \left[\mathbf{D}_{1,1}(n_p)\ \mathbf{D}_{1,2}(n_p)\ \cdots\ \mathbf{D}_{P,Q}(n_p)\right], \quad (54)$$

where $\mathbf{D}(n_p) \in \mathbb{C}^{1\times PQ}$. The range-angle (azimuth) profile (DoA) matrix, $\mathbf{Q} \in \mathbb{C}^{N_c/P\times\Phi}$, is computed by the Frobenius inner product as [8]

$$\mathbf{Q}(n_p,\phi) = \langle\mathbf{D},\mathbf{B}(\phi)\rangle_F, \quad (55)$$

where $\mathbf{B} \in \mathbb{C}^{PQ\times\Phi}$ denotes the beamformer matrix with each column vector defined by

$$\mathbf{B}(\phi) = \left[1\ e^{jsin(\phi)2\pi\frac{d_Q}{\lambda}}\ \cdots\ e^{jsin(\phi)2\pi(PQ-1)\frac{d_Q}{\lambda}}\right]^T. \quad (56)$$

C. Probability of Detection

The probability of detection (P_D) of an arbitrary target under a constant probability of false-alarm (P_{FA}) threshold is also considered as a radar performance metric. The self-interference caused by the direct coupling is assumed completely eliminated by the aforementioned digital canceller, as otherwise, it may cause a constant false-positive target detection. The probability of detection is evaluated based on the range-velocity profile of the single target. To compute the probability of detection, two hypothesis are considered [40]. These hypothesis are $\mathcal{H}_0$, where the return signal includes clutters, noise and reflected communication signals, and $\mathcal{H}_1$, where the return signal includes echos from the target as well as the aforementioned signals. The probability of false-alarm can be obtained by $P_{FA} = Pr\{\mathcal{H}_1;\mathcal{H}_0\}$ and the probability of detection is $P_D = Pr\{\mathcal{H}_1;\mathcal{H}_1\}$ while ensuring the given maximum constant false-alarm rate (CFAR) i.e. $P_{FA} = 10^{-6}$. Lastly, P_D is calculated based on the range-velocity radar images of a single target under downlink communication interference. These images are obtained using the aforementioned range-velocity estimation method via simulations.

VII. Simulations and Numerical Results

In this section, the proposed RadCom architecture is evaluated. QAM OFDM modulated communication downlink is considered under radar interference and CSI errors. PSK waveforms are considered for the radar waveform. RCS of the targets is chosen as $\sigma_u = 0.1$ dBm^2 and the targets are randomly located in the range of 20 m to 200 m in LOS to the BS, in each simulation scenario. The radar operates over L downlink subframes, and thus, the radar processing time is given by $T_{rad} = L\times\Delta t$. Table II summarizes the simulation parameters which are carefully selected to satisfy the radar and communication requirements. For instance, the TDD frame duration is chosen within the channel coherence time by considering the maximum target relative velocity of 200 km/h. Moreover, Table II presents radar performance metrics, such as radar range, velocity and angle resolutions, which are calculated as in [8], [22]. The maximum range of the radar is 200 m as $r_{max} = t_{cp}c_0/2$, and the subcarrier spacing is selected large enough to tolerate the impact of the Doppler shift i.e. $\Delta f \geq 10f_{D_{max}}$, and hence, avoid the subcarrier misalignment [22]. The simulations are averaged over 10^5 random and independent network instances, where the channel conditions vary from one network instance to another.

Fig. 5 illustrates the sum-capacity of 10 UEs when the BS is equipped with 100 antennas and operates with the proposed optimum radar waveform (ORWF) or random radar waveform (RRWF). As benchmarks, the capacity of the ZF without radar interference and under radar interference are given in this figure. It can be seen from Figs. 5a and 5b that the proposed precoder substantially outperforms the ZF as its capacity is significantly degraded by the radar interference. Moreover, RadCom with ORWF can even exceed the achievable capacity of the ZF perocoder when the number of active UEs is less than a certain number depending on the power ratio Ψ. The ZF precoder is significantly affected by the radar interference and is outperformed by the RRWF with imperfect CSI. The capacity gap between ORWF and RRWF gradually increases when the number of UEs grows. It is also observed that imperfect CSI significantly degrades the network capacity especially when the number of UEs increases. The higher radar power restricts the maximum number of UEs that can be served at the same time as seen in Fig. 5a and 5b. These figures also show that the simulation results match the analytical capacity derivations for different values of Ψ, K, and ξ.

Table II
PARAMETERS USED IN SIMULATIONS.

Parameter	Value	Description
f_c	5.8 GHz	Carrier frequency
B	100 MHz	Bandwidth
Δf	114 kHz	OFDM subcarrier spacing
N_c	877	Number of subcarriers
Δt	200 μs	TDD frame duration
t_{sym}	8.77 μs	Elementary symbol duration
t_{cp}	1.33 μs	Cyclic prefix duration
t_o	10 μs	OFDM symbol duration
N_{sym}	10	Symbols in each downlink subframe
L	40	Subframes in each radar waveform
T_{rad}	8 ms	Radar processing time ($L \times \Delta t$)
V	400	Number of radar symbols ($L \times N_{sym}$)
p_{N0}	-174 dBm/Hz	Noise power
G_{tx}, G_{rx}	5 dBi	Receive and transmit antenna gains
z, a	0.3, 0.8	CSI error model parameters
σ_w^2	0.2	Variance of radar clutter
P	2	Number of radar transmit antennas
Q	10	Number of radar receive antennas
r_{max}	200 m	Maximum radar detection range
v_{max}	55.6 m/s	Maximum detectable target velocity
Δr	1.5 m	Radar range resolution
Δv	6.5 m/s	Radar velocity resolution
$\Delta\phi$	5.73°	$P \times Q$ MIMO radar angle resolution
G_p	52.44 dB	OFDM radar processing gain

The impact of increasing radar power output is investigated in Fig. 6 which shows the capacity per UE with 50, 100 and 200 BS antennas when the BS has the perfect CSI knowledge. Having more BS antennas make the communication system robust against a higher radar power output. For example, while it can alleviate the radar interference up to $\Psi = 2$ with $M = 50$ BS antennas, it can support much higher radar output power when more antennas are employed i.e. $\Psi = 8$ with $M = 200$. This figure also shows that the proposed method under radar interference can outperform the ZF precoder which does not have any radar interference with up to $\Psi = 6$. When the radar output power grows, the gap between the simulation and the analytical results widens as cancellation of very high radar output power causes non-linearity in the precoded vector.

Fig. 7 compares the proposed precoder to the shared and separated antenna deployments which were proposed and examined in [13]. In this comparison, the total number of radar and communication antennas is 50, the number of UEs is 5 and the number of targets is 2. While RadCom ORWF and RRWF employ 48 antennas for communication and 2 for emitting omnidirectinal radar waveform, the separated deployment employs 40 antennas for communication and 10 antennas for radar as it needs more radar antennas to perform beamforming towards the targets. The shared deployment uses all of the antennas for transmitting communication data and radar waveform jointly. The communication and radar powers are assumed to be equal to each other i.e. $\Psi = 1$ in all scenarios. It is observed that RadCom ORWF substantially outperforms the other schemes due to employing optimum radar waveforms and utilizing radar interference.

In the previous figures, it was shown that RadCom with ORWF performs significantly better than RRWF. Employing a higher-order PSK modulation scheme might provide more options for the selection of the optimum radar symbol. How-

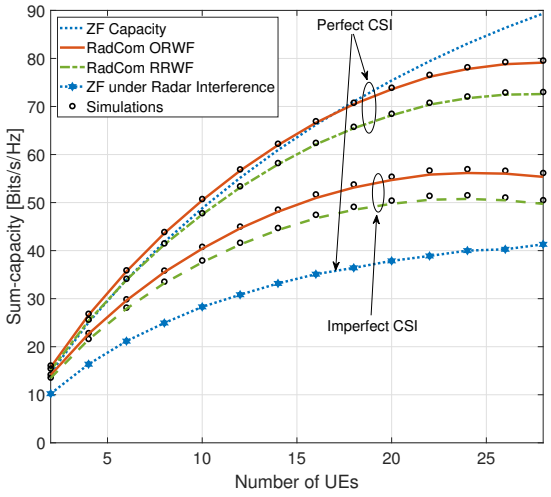

(a) $\Psi = 1$.

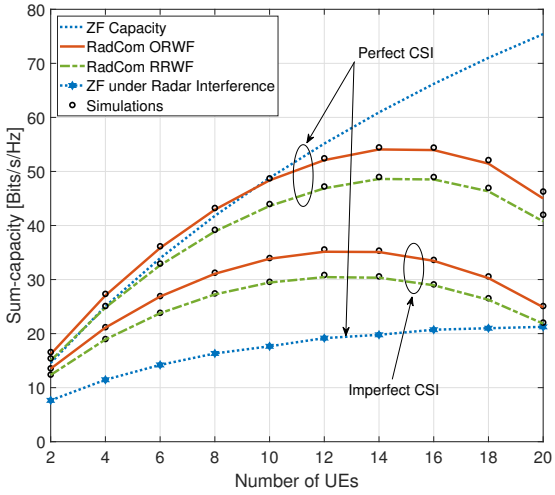

(b) $\Psi = 3$.

Fig. 5. Sum-capacity of the network as a function of number of UEs under radar interference with $\Psi = 1$ and $\Psi = 3$. $K = 10$, $M = 100$, SNR is $\rho = 5$ dB. Channel estimation error parameters $\beta = 0.3$ and $\alpha = 0.8$.

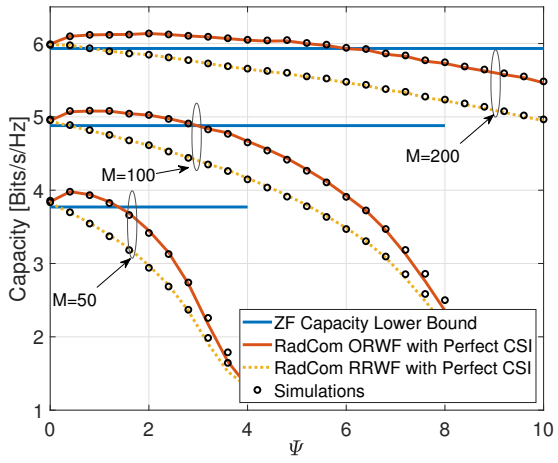

Fig. 6. Capacity of RadCom under various radar-communication power output ratios and number of BS antennas, $K = 10$ and SNR is 5 dB.

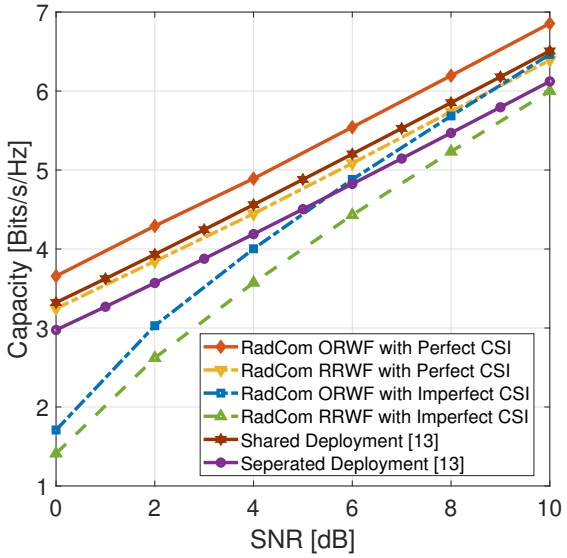

Fig. 7. Capacity per UE of RadCom systems with different methods.

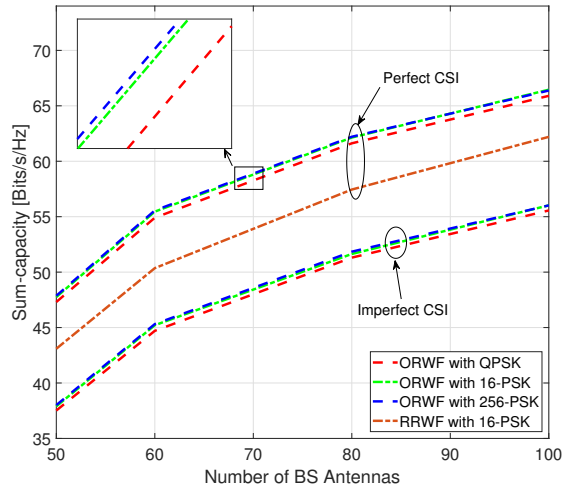

Fig. 8. Performance of different radar waveform modulation schemes.

ever, it may also increase the complexity of radar waveform optimization as it would need to search for the optimum symbol in all possible symbols of the constellation. Fig. 8 illustrates the sum-capacity with different PSK modulation schemes. While the performance gap between QPSK and 16-PSK is significant, the constellations with higher-order (e.g. 256-PSK) than 16-PSK do not provide significantly higher capacity. This can be concluded that 16-PSK allows the selection of near-optimum radar waveform with a reasonably shorter symbol search. This figure also shows that even ORWF with QPSK provides substantially better capacity than RRWF. Besides, having more antennas enhances the capacity of the network with both waveforms even under imperfect CSI.

The radar detection performance of the proposed architecture is evaluated in a scenario where $M = 100$, $K = 10$, $P = 2$, $Q = 10$, and $\Psi = 2$. Two targets (i.e. $U = 2$) are present in the radar range with the same RCS ($\sigma_u = 0.1$ dBm^2). Targets' velocities are -10 m/s and 15 m/s, ranges are 140 m and 90 m, and azimuth angles are -30° and 20°, respectively. The average received SINR of the radar signals received from two targets is -20 dB. However, the processing gain obtained due to the FFT/IFFT operations is $G_p = 52.44$ dB, which is determined using $G_p = VN_c/P$. Particularly, over 40 TDD subframes—within $T_{rad} = 8$ ms of radar processing time—the radar waveform consists of $V = 400$ symbols over $N_c = 877$ active subcarriers. Accordingly, the SINR of the radar images is 32.44 dB, and this substantially reduces the impact of the interference from the communication network. Fig. 9a shows the range-velocity profile of the targets with the impact of the direct-coupling which is seen as a static object very close to the radar in alignment with the previous studies [28]. After estimating this direct-coupling and calibrating the radar to eliminate it, the range-velocity profile presented in Fig. 9b is obtained. It is evident that eliminating the direct-coupling makes the targets more obvious in the radar image. Accordingly, the radar is assumed to be calibrated to completely eliminate the direct-coupling in the next figures. Fig. 9c and Fig. 9d illustrate the azimuth angle estimation of these two targets with the Fourier beamforming method with and without MIMO radar processing, respectively. Applying the MIMO radar processing creates a virtual array with $P \times Q$ elements (i.e. 2×10), and hence, provides a better angle resolution as seen in the comparison of Fig. 9c and Fig. 9d.

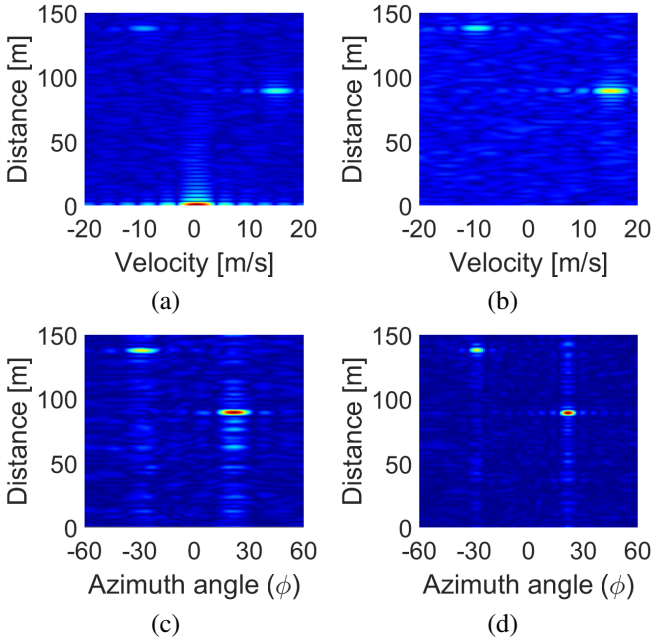

Fig. 9. Estimated range-velocity profiles of two targets: (a) with the direct coupling, (b) after eliminating the direct coupling. Estimated range-angle (azimuth) profiles of the targets using the Fourier beamforming method: (c) without MIMO (d) with MIMO radar processing. $P = 2$, $Q = 10$

Fig. 10 illustrates the trade-off between the communication sum-capacity and radar probability of detection (P_D) while 10 UEs are being served and only one target is being present within 200 m range. In this evaluation, ORWF with 16-PSK is employed as the radar waveform by $P = 2$ radar antennas, and perfect and imperfect CSI situations are considered. The radar-

communication power ratio Ψ is varied between $\Psi = 0$ and $\Psi = 4$ to achieve different radar detection performances and its impact on the sum-capacity is observed. The probability of detection of the radar approaches 1 as the radar output power increases up to $\Psi = 4$ in this specific scenario. It can be seen that the setup with $M = 100$ antennas provides a superior trade-off such that nearly both subsystems can reach their maximum performances without significantly affecting each other if perfect CSI is achieved at the BS. In the case of employing $M = 50$ antennas, the communication capacity should be significantly degraded to achieve a reasonable radar detection accuracy. For instance, in the event of $\Psi = 3.5$, the radar can achieve nearly its maximum detection performance and the sum-capacity of the network with $M = 100$ is still very close to the capacity of the ZF precoder. On the other hand, to achieve a similar detection performance with $M = 50$, the network sum-capacity would be substantially degraded.

The presented analyses and simulation results verify the effectiveness of the proposed precoder for mMIMO OFDM RadCom systems, as it provides a substantial capacity improvement at the cost of a slight increase in system complexity. Moreover, it has been observed that the accuracy of CSI estimation is vital to achieve desirable communication and radar performances. The proposed architecture offers some advantages over employing a single OFDM waveform for radar and communications as in [13], [41]. Firstly, while employing a single OFDM waveform for both functions can be practical in single-input single-output (SISO) systems, it requires prior knowledge of targets or beam-scanning to detect the targets in multi-user scenarios. Because, in multi-user mMIMO systems, the data is beamformed onto the UEs, thus, the transmitted signal power by the BS is not uniform, forming narrow beams towards the UEs with null spaces between them. The proposed architecture enables the detection of the targets omnidirectionally while beamforming data onto UEs. Thus, it does not require any prior knowledge regarding targets or beam-scanning, unlike in [13], [41]. Secondly, it enables detection of several targets at the same time as the target detection is omnidirectional. After estimating the locations of the targets by the proposed architecture, beamforming towards targets can be performed using the methods proposed in [13], [41]. Thirdly, considering that communication systems employ QAM modulations, this can prevent the radar from providing a constant detection performance, since the signal power changes over time in QAM schemes if a single waveform is employed for the both functions. In turn, the proposed architecture satisfies both radar and communication requirements, and allows multi-user communication to substantially improve the communication capacity by transmitting independent waveforms, and exploiting the interference between them to maximize their performance. Lastly, it has been shown that the optimum waveform design improves the communication capacity without affecting the radar performance, since the symbol-based OFDM radar processing is employed.

VIII. Conclusions

This study has presented a dual-functional mMIMO OFDM communication and radar system architecture to communicate with multiple UEs and sense the environment by exploiting the interference between these two systems. It was shown that the interference at the UEs caused by the radar can be entirely utilized while the radar omnidirectionally transmits waveforms which have higher power than the communication signals. Moreover, an optimum OFDM radar waveform design technique is presented to maximize the capacity of the communication network. Mathematical expressions of the communication capacity have been derived under CSI estimation errors and power constraints and verified by simulations. The detection performance of the radar subsystem is also examined under the interference from the communication subsystem, and the trade-off between these systems has been revealed. This study shows that it is possible to develop a transmitter architecture which can satisfactorily communicate with multiple UEs at the same time-frequency resources while sensing the environment, without adding significantly extra cost or complexity to the system. The proposed RadCom architecture can be employed in vehicular or cellular networks to enable joint sensing and communication using the same hardware and the same frequency-time resources.

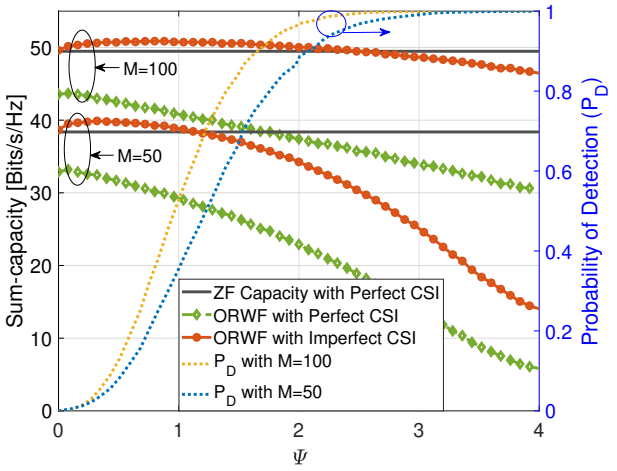

Fig. 10. Communication sum-capacity and radar probability of detection (P_D) under various radar-communication power ratios (Ψ) with $M = 50$ and $M = 100$ BS array elements. $SNR = 5$ dB, $K = 10$ UEs, $p_{FA} = 10^{-6}$.

Appendix

Analytical expressions of the interference caused by CSI errors are derived here. Firstly, the power of the interference from other UEs due to CSI errors can be written as

$$\mathbb{E}\left[\left|\mathbf{e}_{com,k}^{H}\mathbf{w}_{i}^{H}\right|^{2}\right] = \mathbb{E}\left[\left|\mathbf{e}_{com,k}^{H}\mathbf{w}_{i}^{H}\right|\right]^{2} + \mathrm{Var}\left(\mathbf{e}_{com,k}^{H}\mathbf{w}_{i}^{H}\right), \tag{57}$$

where $\mathrm{Var}(.)$ denotes the variance. $\mathbb{E}\left[\left|\mathbf{e}_{com,k}^{H}\mathbf{w}_{i}^{H}\right|\right]^{2} \approx 0$ can be approximately accepted since $\mathbf{e}_{com,k}^{H}$ and $\mathbf{w}_{i}^{H}$ are very slightly correlated. Let $e_{com,k,m}^{*} \in \mathbf{e}_{com,k}^{H}$ and $w_{i,m}^{*} \in \mathbf{w}_{i}^{H}$ denote the mth elements of the corresponding vectors. Accordingly, the following approximation can be given

$$\mathrm{Var}\left(\mathbf{e}_{com,k}^{H}\mathbf{w}_{i}^{H}\right) \approx \sum_{m=1}^{M} \mathrm{Var}\left(e_{com,k,m}^{*}\right) \mathrm{Var}\left(w_{i,m}^{*}\right) \quad (58)$$

$$\approx M\mathrm{Var}\left(e_{com,k,m}^{*}\right) \mathrm{Var}\left(w_{i,m}^{*}\right), \quad (59)$$

where $\mathrm{Var}\left(e_{com,k,m}^{*}\right) = \xi$ and $\mathrm{Var}\left(w_{i,m}^{*}\right) = \frac{1}{M(M-K)}$. Hence,

$$\mathbb{E}\left[\left|\mathbf{e}_{com,k}^{H}\mathbf{w}_{i}^{H}\right|^{2}\right] \approx \frac{\xi}{M-K}. \quad (60)$$

In the same manner, $\mathbb{E}\left[\left|\mathbf{e}_{com,k}^{H}\mathbf{w}_{k}^{H}\right|^{2}\right]$ can also be explicitly written as (57), however, this time $\mathbb{E}\left[\left|\mathbf{e}_{com,k}^{H}\mathbf{w}_{k}^{H}\right|\right]^{2} = \xi^{2}$ due to the strong correlation between $\mathbf{e}_{com,k}^{H}$ and $\mathbf{w}_{k}^{H}$, and $\mathrm{Var}\left(\mathbf{e}_{com,k}^{H}\mathbf{w}_{k}^{H}\right)$ is the same as given by (60), hence, the following expression is obtained,

$$\mathbb{E}\left[\left|\mathbf{e}_{com,k}^{H}\mathbf{w}_{k}^{H}\right|^{2}\right] \approx \xi^{2} + \frac{\xi}{M-K}. \quad (61)$$

ACKNOWLEDGEMENT

This work was partially supported by the Kuwait Foundation for the Advancement of Sciences (KFAS), under project code PN17-15EE-02.

REFERENCES

[1] M. Kalil, A. Al-Dweik, M. F. Abu Sharkh, A. Shami, and A. Refaey, "A framework for joint wireless network virtualization and cloud radio access networks for next generation wireless networks," *IEEE Access*, vol. 5, pp. 20 814–20 827, 2017.

[2] P. Kumari, J. Choi, N. Gonzalez-Prelcic, and R. W. Heath, "IEEE 802.11ad-based radar: An approach to joint vehicular communication-radar system," *IEEE Trans. Veh. Technol.*, vol. 67, no. 4, pp. 3012–3027, 2018.

[3] S. Sodagari, A. Khawar, T. C. Clancy, and R. McGwier, "A projection based approach for radar and telecommunication systems coexistence," in *Proc. of IEEE Global Communications Conference (GLOBECOM)*, Dec 2012, pp. 5010–5014.

[4] A. Khawar, A. Abdel-Hadi, and T. C. Clancy, "Spectrum sharing between S-band radar and LTE cellular system: A spatial approach," in *Proc. of IEEE International Symposium on Dynamic Spectrum Access Networks (DYSPAN)*, Apr. 2014, pp. 7–14.

[5] J. A. Mahal, A. Khawar, A. Abdelhadi, and T. C. Clancy, "Spectral coexistence of MIMO radar and MIMO cellular system," vol. 53, no. 2, pp. 655–668, Apr. 2017.

[6] B. Li and A. P. Petropulu, "Joint transmit designs for coexistence of MIMO wireless communications and sparse sensing radars in clutter," *IEEE Trans. Aerosp. Electron. Syst.*, vol. 53, no. 6, pp. 2846–2864, Dec. 2017.

[7] M. Labib, V. Marojevic, A. F. Martone, J. H. Reed, and A. I. Zaghloui, "Coexistence between communications and radar systems: A survey," *URSI Radio Science Bulletin*, vol. 2017, no. 362, pp. 74–82, Sept. 2017.

[8] Y. L. Sit, B. Nuss, and T. Zwick, "On mutual interference cancellation in a MIMO OFDM multiuser radar-communication network," *IEEE Trans. Veh. Technol.*, vol. 67, no. 4, pp. 3339–3348, Apr. 2018.

[9] B. Hong, W. Wang, and C. Liu, "Ergodic interference alignment for spectrum sharing radar-communication systems," *IEEE Trans. Veh. Technol.*, vol. 68, no. 10, pp. 9785–9796, Oct. 2019.

[10] C. Shi, F. Wang, M. Sellathurai, J. Zhou, and S. Salous, "Power minimization-based robust OFDM radar waveform design for radar and communication systems in coexistence," *IEEE Trans. Signal Process.*, vol. 66, no. 5, pp. 1316–1330, Mar. 2018.

[11] F. Liu, C. Masouros, A. Li, T. Ratnarajah, and J. Zhou, "MIMO radar and cellular coexistence: A power-efficient approach enabled by interference exploitation," *IEEE Trans. Signal Process.*, vol. 66, no. 14, pp. 3681–3695, Jul. 2018.

[12] B. Paul, A. R. Chiriyath, and D. W. Bliss, "Survey of RF communications and sensing convergence research," *IEEE Access*, vol. 5, pp. 252–270, 2017.

[13] F. Liu, C. Masouros, A. Li, H. Sun, and L. Hanzo, "MU-MIMO communications with MIMO radar: From co-existence to joint transmission," *IEEE Trans. Wireless Commun.*, vol. 17, no. 4, pp. 2755–2770, Apr. 2018.

[14] F. Liu, L. Zhou, C. Masouros, A. Li, W. Luo, and A. Petropulu, "Toward dual-functional radar-communication systems: Optimal waveform design," *IEEE Trans. Signal Process.*, vol. 66, no. 16, pp. 4264–4279, Aug. 2018.

[15] J. A. Zhang, X. Huang, Y. J. Guo, J. Yuan, and R. W. Heath, "Multibeam for joint communication and radar sensing using steerable analog antenna arrays," *IEEE Trans. Veh. Technol.*, vol. 68, no. 1, pp. 671–685, Jan. 2019.

[16] X. Wang, A. Hassanien, and M. G. Amin, "Dual-function MIMO radar communications system design via sparse array optimization," *IEEE Trans. Aerosp. Electron. Syst.*, vol. 55, no. 3, pp. 1213–1226, Jun. 2019.

[17] C. Shi, F. Wang, S. Salous, and J. Zhou, "Joint subcarrier assignment and power allocation strategy for integrated radar and communications system based on power minimization," *IEEE Sensors J.*, vol. 19, no. 23, pp. 11 167–11 179, 2019.

[18] C. Shi, F. Wang, M. Sellathurai, J. Zhou, and S. Salous, "Low probability of intercept-based optimal power allocation scheme for an integrated multistatic radar and communication system," *IEEE Syst. J.*, vol. 14, no. 1, pp. 983–994, 2020.

[19] Y. Zhou, H. Zhou, F. Zhou, Y. Wu, and V. C. M. Leung, "Resource allocation for a wireless powered integrated radar and communication system," *IEEE Wireless Commun. Lett.*, vol. 8, no. 1, pp. 253–256, 2019.

[20] E. G. Larsson, O. Edfors, F. Tufvesson, and T. L. Marzetta, "Massive MIMO for next generation wireless systems," *IEEE Commun. Mag.*, vol. 52, no. 2, pp. 186–195, Feb. 2014.

[21] M. Temiz, E. Alsusa, and L. Danoon, "A receiver architecture for dual-functional massive MIMO OFDM RadCom systems," in *2020 IEEE International Conference on Communications Workshops (ICC Workshops)*, June 2020, pp. 1–6.

[22] C. Sturm and W. Wiesbeck, "Waveform design and signal processing aspects for fusion of wireless communications and radar sensing," *Proc. IEEE*, vol. 99, no. 7, pp. 1236–1259, Jul. 2011.

[23] J. Li and P. Stoica, "MIMO radar with colocated antennas," *IEEE Signal Process. Mag.*, vol. 24, no. 5, pp. 106–114, Sept. 2007.

[24] C. Sturm, Y. L. Sit, M. Braun, and T. Zwick, "Spectrally interleaved multi-carrier signals for radar network applications and multi-input multi-output radar," *IET Radar, Sonar Navigation*, vol. 7, no. 3, pp. 261–269, Mar. 2013.

[25] C. Baquero Barneto, T. Riihonen, M. Turunen, L. Anttila, M. Fleischer, K. Stadius, J. Ryynanen, and M. Valkama, "Full-duplex OFDM radar with LTE and 5G NR waveforms: Challenges, solutions, and measurements," *IEEE Trans. Microw. Theory Techn.*, vol. 67, no. 10, pp. 4042–4054, Oct. 2019.

[26] G. Zheng, "DOA estimation in MIMO radar with non-perfectly orthogonal waveforms," *IEEE Commun. Lett.*, vol. 21, no. 2, pp. 414–417, Feb. 2017.

[27] M. Temiz, E. Alsusa, L. Danoon, and Y. Zhang, "On the impact of antenna array geometry on indoor wideband massive MIMO networks," *IEEE Trans. Antennas Propag.*, pp. 1–1, 2020.

[28] B. Nuss, L. Sit, M. Fennel, J. Mayer, T. Mahler, and T. Zwick, "MIMO OFDM radar system for drone detection," in *Proc. of 18th International Radar Symposium (IRS)*, 2017, pp. 1–9.

[29] X. Chen, S. Zhang, and Q. Li, "A review of mutual coupling in MIMO systems," *IEEE Access*, vol. 6, pp. 24 706–24 719, 2018.

[30] M. Mowlér, B. Lindmark, E. G. Larsson, and B. Ottersten, "Joint estimation of mutual coupling, element factor, and phase center in antenna arrays," *EURASIP Journal on Wireless Communications and Networking*, vol. 2007, pp. 1–9, 2007.

[31] M. Temiz, E. Alsusa, and L. Danoon, "Impact of imperfect channel estimation and antenna correlation on quantised massive multiple-input multiple-output systems," *IET Communications*, vol. 13, no. 9, pp. 1262–1270, 2019.

[32] P. Aquilina and T. Ratnarajah, "Performance analysis of IA techniques in the MIMO IBC with imperfect CSI," *IEEE Trans. Commun.*, vol. 63, no. 4, pp. 1259–1270, Apr. 2015.

[33] D. Mi, M. Dianati, L. Zhang, S. Muhaidat, and R. Tafazolli, "Massive MIMO performance with imperfect channel reciprocity and channel estimation error," *IEEE Trans. Commun.*, vol. 65, no. 9, pp. 3734–3749, Sept. 2017.

[34] C. Masouros, T. Ratnarajah, M. Sellathurai, C. B. Papadias, and A. K. Shukla, "Known interference in the cellular downlink: a performance limiting factor or a source of green signal power?" *IEEE Commun. Mag.*, vol. 51, no. 10, pp. 162–171, Oct. 2013.

[35] H. Q. Ngo, E. G. Larsson, and T. L. Marzetta, "Energy and spectral efficiency of very large multiuser MIMO systems," *IEEE Trans. Commun.*, vol. 61, no. 4, pp. 1436–1449, Apr. 2013.
[36] C. Sturm, T. Zwick, W. Wiesbeck, and M. Braun, "Performance verification of symbol-based OFDM radar processing," in *Proc. of IEEE Radar Conference*, 2010, pp. 60–63.
[37] R. Hunger, "Floating point operations in matrix-vector calculus," Associate Institute for Signal Processing, The Technical University of Munich, Tech. Rep. v1.3, September 2007. [Online]. Available: https://mediatum.ub.tum.de/doc/625604/625604
[38] C. Zhang, Y. Jing, Y. Huang, and L. Yang, "Performance analysis for massive MIMO downlink with low complexity approximate zero-forcing precoding," *IEEE Trans. Commun.*, vol. 66, no. 9, pp. 3848–3864, 2018.
[39] M. Braun, R. Tanbourgi, and F. K. Jondral, "Co-channel interference limitations of OFDM communication-radar networks," *EURASIP Journal on Wireless Communications and Networking*, 2013, article no. 207.
[40] J. R. Krier, M. C. Norko, J. T. Reed, R. J. Baxley, A. D. Lanterman, Xiaoli Ma, and J. R. Barry, "Performance bounds for an OFDM-based joint radar and communications system," in *Proc. of IEEE Military Communications Conference (MILCOM)*, Oct. 2015, pp. 511–516.
[41] M. L. Rahman, J. A. Zhang, X. Huang, Y. J. Guo, and R. W. Heath, "Framework for a perceptive mobile network using joint communication and radar sensing," *IEEE Trans. Aerosp. Electron. Syst.*, vol. 56, no. 3, pp. 1926–1941, June 2020.

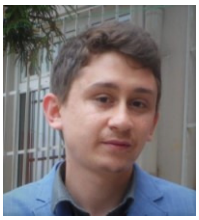

Murat Temiz (S'19) received B.S. degree in Electronics and Computer Science with Education from Gazi University and M.S. degree in Electrical and Electronics Engineering from TOBB University of Economics and Technology, respectively, both in Ankara, Turkey. He is currently a Ph.D. student and a research assistant in the Department of Electrical and Electronic Engineering, the University of Manchester, UK. His current research interests are massive MIMO systems, antenna and antenna array design, channel measurements, optimization, dual-functional MIMO OFDM radar-communication systems and machine learning applications. He has published several publications in top IEEE journals and conferences.

Emad Alsusa (M'06-SM'07) completed a PhD in Telecommunications from the University of Bath in the United Kingdom in 2000 and in the same year he was appointed to work on developing high data rates systems as part of an industrial project based at Edinburgh University. He joined Manchester University (then UMIST) in September 2003 as a faculty member where his current rank is a Reader in the Communication Engineering Group. His research interests lie in the area of Communication Systems with a focus on Physical, MAC and Network Layers including developing techniques and algorithms for array signal detection, channel estimation and equalization, adaptive signal precoding, interference avoidance through novel radio resource management techniques, cognitive radio and energy and spectrum optimization techniques. Applications of his research include cellular networks, IoT, Industry 4.0, and Powerline Communications. Emad's research work has resulted in over 200 journals and refereed conference publications mainly in top IEEE transactions and conferences. Emad has supervised over 25 PhDs to successful completion. Emad is an Editor of the IEEE Wireless communication Letters, a Fellow of the UK Higher Academy of Education, and a TPC Track Chair of a number of conferences such as VTC'16, GISN'16, PIMRC'17 and Globecom'18, as well as the General Co-Chair of the OnlineGreenCom'16 Conference. He is currently the UK representative in the International Union of Radio Science, and a Co-Chair of the IEEE Special Working Group on RF Energy Harvesting. Emad has received a number of awards including the best paper award in the international Symposium on Power Line Communications 2016 and the Wireless Communications and Networks Conference 2019.

Mohammed W. Baidas (M'05-SM'17) received the B.Eng. (Hons.) degree in communication systems engineering from the University of Manchester, Manchester, U.K., in 2005, the M.Sc. degree (with distinction) in wireless communications engineering from the University of Leeds, Leeds, U.K., in 2006, the M.S. degree in electrical engineering from the University of Maryland, College Park, MD, USA, in 2009, and the Ph.D. degree in electrical engineering from Virginia Tech, Blacksburg, VA, USA, in 2012. Dr. Baidas was a Visiting Researcher with the University of Manchester in the academic years of 2015/2016 and 2018/2019. He is currently an Associate Professor with the Department of Electrical Engineering, Kuwait University, Kuwait, where he has been on the faculty since May 2012. He is also a frequent reviewer for several IEEE journals and international journals and conferences, with over 70 publications. His research interests include resource allocation and management in cognitive radio systems, game theory, cooperative communications and networking, and green and energy-harvesting networks. He also serves as a technical program committee member for various IEEE and international conferences. He was a recipient of the Outstanding Teaching Award of Kuwait University for the academic year of 2017/2018.